Journal of Asian Earth Sciences 79 (2014) 884–894

Contents lists available at SciVerse ScienceDirect

Journal of Asian Earth Sciences

journal homepage: www.elsevier.com/locate/jseaes

Origin of the ore-forming fluids of the Tongchang porphyry Cu–Mo deposit in the Jinshajiang–Red River alkaline igneous belt, SW China: Constraints from He, Ar and S isotopes

Leiluo Xu [a], Xianwu Bi [a,*], Ruizhong Hu [a], Yongyong Tang [a,b], Guohao Jiang [a], Youqiang Qi [a]

[a] State Key Laboratory of Ore Deposit Geochemistry, Institute of Geochemistry, Chinese Academy of Sciences, Guiyang 550002, China
[b] Graduate University of Chinese Academy of Sciences, Beijing 100049, China

ARTICLE INFO

Article history:
Available online 27 February 2013

Keywords:
He
Ar and S isotopes
Origin of the ore-forming fluid
Tongchang deposit
Jinshajiang–Red River alkaline igneous belt

ABSTRACT

The Jinshajiang–Red River alkaline igneous belt with abundant Cu–Mo–Au mineralization, in the eastern Indian–Asian collision zone, is an important Cenozoic magmatic belt formed under an intra-continental strike-slip system in southwestern (SW) China. The Tongchang deposit is a representative porphyry Cu–Mo deposit in southern segment of the Jinshajiang–Red River alkaline igneous belt, with 8621 t Cu @ 1.24 wt.% and 17,060 t Mo @ 0.218 wt.%. In this study, He, Ar and S isotopic compositions of the Tongchang deposit were determined. He and Ar isotopic compositions suggest that the ore-forming fluids, with $^{3}He/^{4}He$ ratios varying from 0.17 to 1.50 Ra and $^{40}Ar/^{36}Ar$ ratios from 299.1 to 347.3 for the deposit, are a mixture between a crust-derived fluid (MASW) with near atmospheric Ar and crustal He, and a mantle-derived fluid. However, the $\delta^{34}S$ values of the hydrothermal pyrite samples ranging from 1.0‰ to 1.5‰ with an average of 1.2‰, indicate that the sulfur in the ore-forming fluids of the Tongchang deposit was primarily derived from the magma or indirectly mantle-derived without assimilation of crustal sulfur. In combination with previously published He and Ar isotopic data of the Yulong and Machangqing deposits in northern and central segments of the Jinshajiang–Red River alkaline igneous belt, respectively, the ore-forming fluids of the Yulong and Machangqing deposits are obviously richer in ^{3}He and ^{40}Ar, and poorer in ^{36}Ar in comparison with the Tongchang deposit, implying that more mantle-derived fluids were involved in the ore-forming fluids of the Yulong and Machangqing deposits than those for the Tongchang deposit. This might be one of the most important factors producing larger scales of mineralization in the Yulong and Machangqing deposits than the Tongchang deposit.

1. Introduction

Alkaline igneous rocks are a special type of rock with combined potassium and sodium contents high enough to be plotted in or above the basanite, trachybasalt, shoshonite, latite and trachyte fields in the IUGS classification scheme for volcanic rocks (Sillitoe, 2002). These rocks are considered to be formed in four principal tectonic settings: continental arcs, post-collisional arcs, oceanic arcs and within-plate, and were all mantle-derived (Müller and Groves, 2000). Due to their relationships with various types of mineralization, e.g., porphyry Cu–Au, skarn Cu–Au, sediment-hosted (Carlin-style) Au, breccia pipe, low-sulfidation epithermal Au, pluton-related (mesothermal or orogenic) Au vein and volcanogenic massive sulfide deposits, and their importance in reconstructing the tectonic setting of ancient terranes into which they were intruded, these rocks have recently attracted much attention among geoscientists worldwide (Müller and Groves, 2000; Müller et al., 2002; Sillitoe, 2002). As a result, a special issue in Mineralium Deposita (Volume 37 in 2002) were published to discuss this type of rock and associated mineralization.

The Jinshajiang–Red River alkaline igneous belt, extending over 2000 km long in the eastern Indian–Asian collision zone, is an important Cenozoic magmatic belt formed in an intra-continental strike-slip system in SW China (Fig. 1; Hou et al., 2003; Hu et al., 2004). This belt has played a vital role in understanding the tectonic evolution of Cenozoic age in this region and has been a subject of numerous studies (Tapponnier et al., 1982; Schärer et al., 1990, 1994; Leloup et al., 1993, 1995, 2001; Turner et al., 1993a,b, 1996; Chung et al., 1997, 1998). From 1960s, a series of porphyry Cu–Mo deposits (Fig. 1; e.g., the Yulong, Machangqing and Tongchang deposits, etc.) and epithermal Au deposits (e.g., the Beiya and Yao'an deposits, etc.) were discovered successively in the Jinshajiang–Red River alkaline igneous belt, making it an

* Corresponding author. Tel.: +86 851 5891962; fax: +86 851 5891664.
E-mail address: bixianwu@vip.gyig.ac.cn (X. Bi).

1367-9120/$ - see front matter © 2013 Elsevier Ltd. All rights reserved.
http://dx.doi.org/10.1016/j.jseaes.2013.02.013

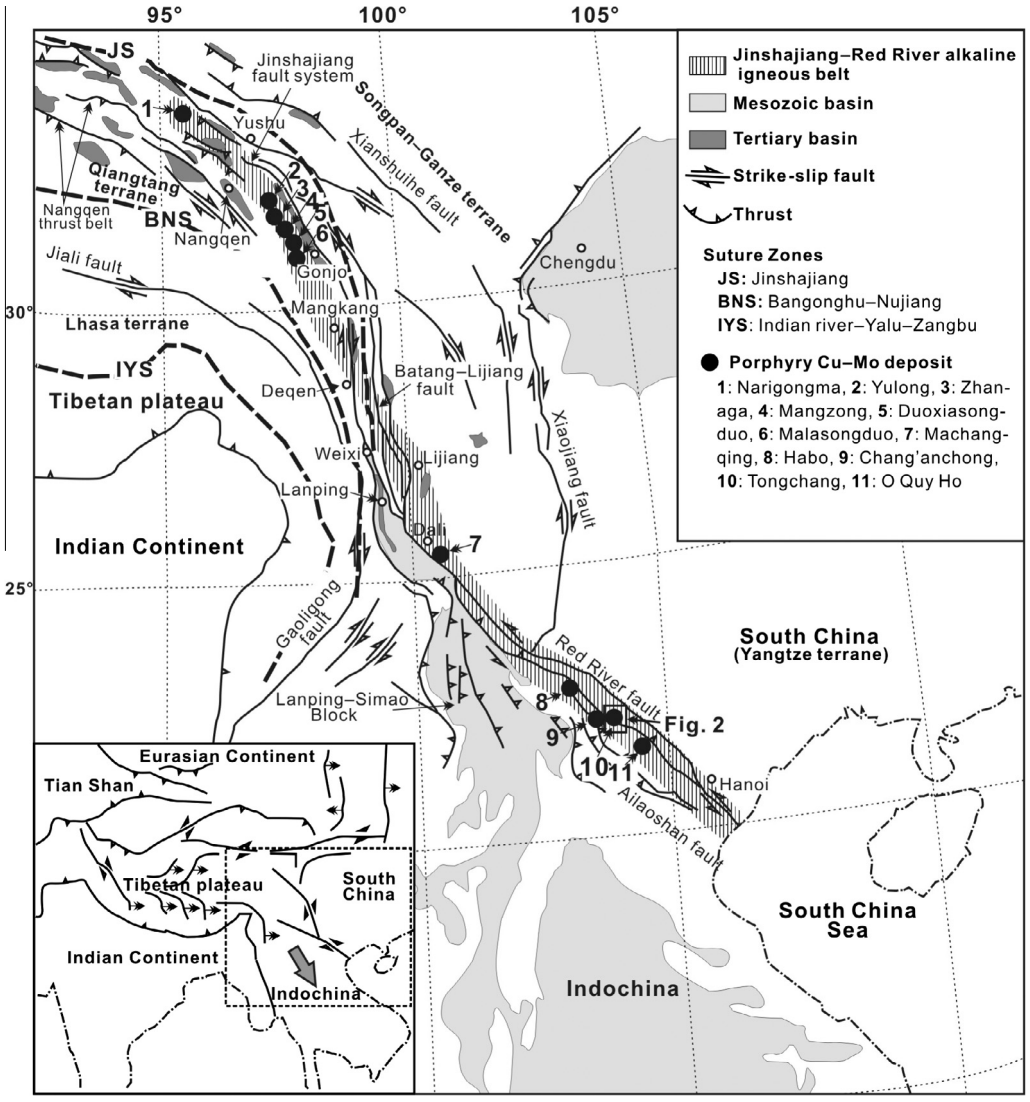

Fig. 1. Simplified geological map showing the Cenozoic tectonic framework and the distribution of porphyry Cu–Mo deposits in the Jinshajiang–Red River alkaline igneous belt (modified from Wang et al. (2001)).

important area of widespread Cu–Mo–Au mineralization of Cenozoic age in SW China (Hu et al., 1998, 2004; Hou et al., 2003, 2007a).

The Tongchang deposit is a representative porphyry Cu–Mo deposit in southern segment of the Jinshajiang–Red River alkaline igneous belt (Fig. 1), with 8621 t Cu @ 1.24 wt.% and 17,060 t Mo @ 0.218 wt.% (Xu et al., 2011). Compared with the representative porphyry Cu–Mo deposits (Fig. 1; e.g., the Yulong deposit in north with 6.5 Mt Cu @ 0.38 wt.%, 0.15 Mt Mo @ 0.04 wt.%, and the Machangqing deposit in central segment with 0.25 Mt Cu @ 0.44 wt.%) in central and northern segments of the Jinshajiang–Red River alkaline igneous belt, the deposits (Fig. 1; e.g., the Tongchang deposit and the Chang'anchong deposit with 29,337 t Cu @ 1.48 wt.% and 13,310 t Mo @ 0.13 wt.%) in southern segment of the belt usually have relatively small scales of mineralization (Xu et al., 2012). In addition, recent studies revealed some remarkable differences in the magmatic sources, and ages of magmatic emplacement and mineralization for the Tongchang, Machangqing and Yulong porphyry Cu–Mo deposits, in southern, central and northern segments of the belt, respectively (Table 1; Hu et al., 2004; Hou et al., 2006; Xu et al., 2011, 2012). The above-mentioned differences provide significant help for better understanding the characteristics of the porphyry Cu–Mo mineralization in the Jinshajiang–Red River alkaline igneous belt. The origins of the ore-forming fluids of the Machangqing and Yulong deposits have been investigated by previous studies (Hu et al., 1998, 2004; Bi et al., 1999; Gu et al., 2003; Hou et al., 2007b). However, few definitive studies were conducted on the characteristics of the ore-forming fluids of the porphyry Cu–Mo deposits located in southern segment of the belt, especially a systematic comparison of the ore-forming fluids among the porphyry Cu–Mo deposits with different scales of mineralization in this belt. Thus, a systematic study on the ore-forming fluids of the porphyry Cu–Mo deposits in the Jinshajiang–Red River alkaline igneous belt will shed new light on the mechanisms of associated porphyry Cu–Mo mineralization in this belt.

The compositions of noble gases (e.g. He and Ar, etc.) in various geochemical reservoirs (e.g. crust and mantle, etc.) have notable differences and show a unique advantage in tracing the sources of ore-forming fluids (Simmons et al., 1987; Turner and Stuart, 1992; Turner et al., 1993a,b; Stuart et al., 1995; Burnard et al., 1999; Hu et al., 1998, 1999, 2004, 2009, 2012; Li et al., 2007, 2010, 2011; Sun et al., 2009; Wu et al., 2011; Burnard, 2012). This is because $^{40}Ar/^{36}Ar$ ratios can clearly exhibit the difference about atmospheric versus crust or mantle Ar, and the $^{3}He/^{4}He$ ratios of mantle-derived fluids can reach 1000 times higher than those of

Table 1
Geological and mineralization characteristics of some representative alkaline intrusion-related porphyry Cu–Mo deposits in the Jinshajiang–Red River alkaline igneous belt.

Deposit	Yulong	Machangqing	Tongchang
Wall rock	T_3: crystalline limestone	O_1–D_1: limestone and sandstone	S_2: limestone and sandstone
Intrusion type	Monzogranite porphyry	Granite porphyry	Quartz syenite porphyry
Occurence	Stocks	Stocks	Stocks and dykes
Outcrop area	0.64 km^2	1.3 km^2	0.20 km^2
Mineral assemblage[a]	Kfs + Pl + Q + Hb + Bi	Kfs + Pl + Q + Hb + Bi	Kfs + Pl + Q + Hb + Bi
Chemical composition	SiO_2 = 67.60–70.90 wt.%	SiO_2 = 69.37–72.81 wt.%	SiO_2 = 63.22–68.90 wt.%
	CaO = 0.77–2.21 wt.%	CaO = 0.88–2.21 wt.%	CaO = 1.04–3.82 wt.%
	$K_2O + Na_2O$ = 8.07–9.82 wt.%	$K_2O + Na_2O$ = 8.06–9.74 wt.%	$K_2O + Na_2O$ = 9.21–10.47 wt.%
	K_2O/Na_2O = 2.28–3.10	K_2O/Na_2O = 0.91–2.45	K_2O/Na_2O = 1.01–1.44
	A/CNK = 1.02–1.11	A/CNK = 0.87–1.11	A/CNK = 0.77–1.05
	REE = 130–304 ppm	REE = 214–258 ppm	REE = 331–408 ppm
	$(La/Yb)_N$ = 31–51	$(La/Yb)_N$ = 27–34	$(La/Yb)_N$ = 38–61
	I_{Sr} = 0.706449–0.707009	I_{Sr} = 0.705303–0.707238	I_{Sr} = 0.707093–0.707133
	$\varepsilon_{Nd}(t)$ = −2.8 to −2.4	$\varepsilon_{Nd}(t)$ = −6.5 to −3.4	$\varepsilon_{Nd}(t)$ = −7.1 to −6.8
Intrusion age	43.8–38.9 Ma (zircon U–Pb)	36.2–35.0 Ma (zircon U–Pb)	35.8–34.6 Ma (zircon U–Pb)
Mineralization age	41.6–40.1 Ma (molybdenite Re–Os)	35.8–33.9 Ma (molybdenite Re–Os)	34.4–34.0 Ma (molybdenite Re–Os)
Alteration zoning	K-silicate → quartz–sericite → propylitic → argillic → skarn	K-silicate → quartz–sericite → advanced argillic → skarn	K-silicate → quartz–sericite → skarn
Mineralization	Cu–Mo–Au	Cu–Mo–Au	Cu–Mo–Au
Tonnage, grade	6.5 Mt Cu (0.38 wt.%), 0.15 Mt Mo (0.04 wt.%), 0.35 ppm Au	0.25 Mt Cu (0.44 wt.%), 0.03 wt.% Mo, 0.03 ppm Au	8621 t Cu (1.24 wt.%), 17,060 t Mo (0.218 wt.%), 0.13 ppm Au
Ore structure	Veinlet, disseminated, massive	Veinlet, disseminated, massive	Veinlet, disseminated, massive
Orebody shape	Stratiform and lenticular orebody in stock and contact	Lenticular, pocket, and irregular orebody in stock	Stratiform and lenticular orebody in stock and skarn

Data are mainly from Hou et al. (2003), Hu et al. (2004), Jiang et al. (2006), Liang et al. (2006a,b), Bi et al. (2009), Xu (2011) and Xu et al. (2011, 2012).
[a] Mineral symbol: Kfs = K-feldspar; Pl = plagioclase; Q = quartz; Hb = hornblende; Bi = biotite.

crust-derived fluids, and moreover, even minor mantle-derived He in the ore-forming fluids can be identified by He isotope results (Stuart et al., 1995; Hu et al., 1998, 1999, 2004, 2009, 2012; Sun et al., 2009). Thus, He and Ar isotopes can provide a unique insight into processes in which mantle volatiles have been added to crustal fluids.

In the present study, He, Ar and S isotopic compositions of the Tongchang porphyry Cu–Mo deposit were reported. Combined with previous published He and Ar isotopic data of the Machangqing and Yulong deposits (Hu et al., 1998, 2004), we constrain the origin of the ore-forming fluids of the Tongchang porphyry Cu–Mo deposit and evaluate the possible differences between the Tongchang, Machangqing and Yulong deposits.

2. Regional background and geology of the Tongchang deposit

The Jinshajiang–Red River alkaline igneous belt is adjacent to the NNW–NW-trending Jinshajiang–Red River deep fault zone in the eastern Indo–Asian collision zone. The eastern Indo–Asian collision zone comprises several terranes: from north to south, the Songpan–Ganze, Qiangtang, Lhasa and Yangtze terranes, which were welded together prior to the Cretaceous to form part of the Eurasian plate (Fig. 1). From ca. 70 to 60 Ma, the Indo–Asian collision created the Tibetan plateau and resulted in northeastward extrusion tectonics facilitated by strike-slip motion along a series of strike-slip faults. The strike-slip motion along the Jinshajiang–Red River deep fault caused lithospheric-scale extension and emplacement of numerous alkaline igneous rocks including volcanic and intrusive rocks, forming an over 2000 km-long and generally 50–80 km-wide Jinshajiang–Red River alkaline magmatic belt (Zhang et al., 1987; Turner et al., 1996; Chung et al., 1997, 1998; Bi, 1999; Bi et al., 1999, 2002, 2004, 2005, 2009; Yin and Harrison, 2000; Hou et al., 2006, 2007a,b,c). Zircon U–Pb dating indicates that these alkaline igneous rocks have ages ranging between ca. 43 Ma and ca. 35 Ma (Xu, 2011; Xu et al., 2012). These alkaline igneous rocks range from basaltic to trachytic and rhyolitic in chemical composition (Chung et al., 1998). They are characterized by high alkali ($K_2O + Na_2O > 8$ wt.%) and enrichment in potassium ($K_2O/Na_2O > 1$) belonging to high-K calc-alkaline and shoshonitic series, and exhibit incompatible trace-element patterns with highly enriched large-ion lithophile elements and light rare-earth elements, and marked depletions in the high field strength elements, such as Nb, Ta and Ti (Chung et al., 1998; Hou et al., 2003; Bi et al., 2005). The Sr–Nd isotopic compositions of these alkali-rich igneous rocks (Zhang and Xie, 1997; Hou et al., 2003; Bi et al., 2005; Jiang et al., 2006) suggest the origination from an enriched mantle source (EMII). Rock types of the alkaline intrusions associated with porphyry Cu–Mo mineralization mainly consist of monzogranite porphyry, granite porphyry and syenite porphyry.

The Tongchang deposit is situated in southern segment of the Jinshajiang–Red River alkaline igneous belt (Fig. 1). It was discovered in 1950s, and then explored firstly by No. 15 Geological Survey Team of Yunan Geological Bureau in 1970s. The deposit was estimated to contain about 8621 t Cu @ 1.24 wt.%, 17,060 t Mo @ 0.218 wt.% and 0.13 ppm Au (Xue, 2008). Three stages of magmatisms occurred in the Tongchang orefield, including the early stage of fine-grained syenites, middle stage of quartz syenite porphyries, and late stage of syenite porphyries, diabases and diabase gabrros (Fig. 2). The Cu–Mo-mineralization primarily occurs within and around the middle stage of quartz syenite porphyries (mainly No. 2 quartz syenite porphyry intrusion; Fig. 2) with a zircon U–Pb age of ca. 35 Ma (Huang et al., 2009; Xu et al., 2012) in the Tongchang orefield. The molybdenite Re–Os age of ca. 34 Ma (Xu et al., 2012) for the Tongchang deposit indicates that the Cu–Mo-mineralization was closely related to the quartz

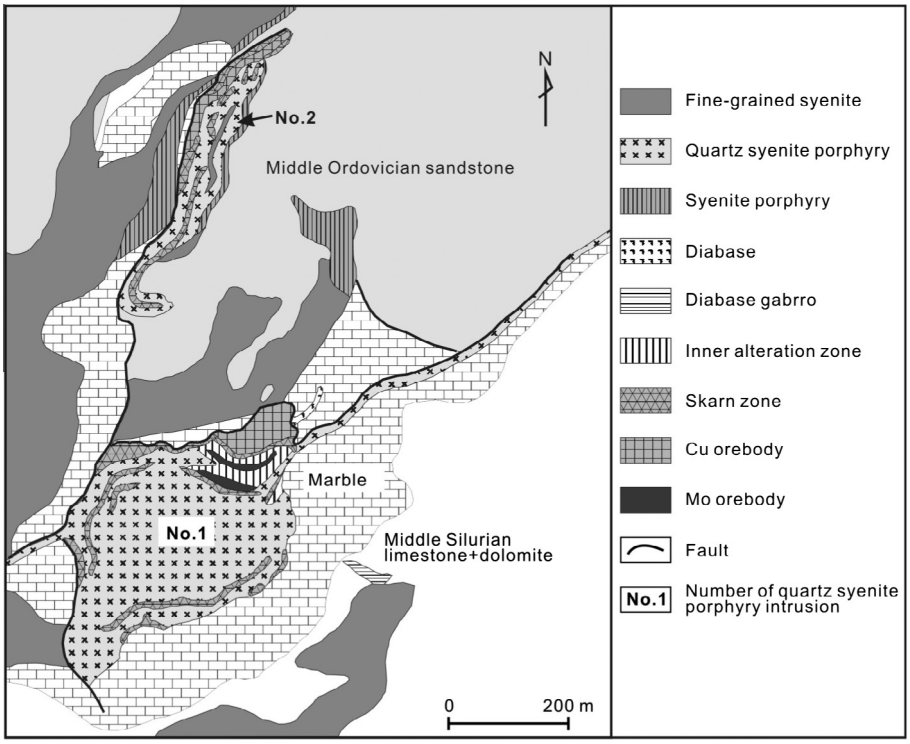

Fig. 2. Simplified geological map of the Tongchang deposit (modified from No. 15 Geological Survey Team of Yunan Geological Bureau (1973)).

syenite porphyries. The light-pink quartz syenite porphyry exhibits massive structure and porphyritic texture, with phenocrysts of K-feldspar (50–60%), plagioclase (20–30%), quartz (10–15%), hornblende (5–10%) and biotite (1–5%) in a phanerocrystalline matrix with similar mode. The accessory minerals are dominated by apatite, zircon and titanite. Three notable alteration zones (i.e., inner alteration zone, skarn zone and outer alteration zone) have been identified from the inner part of the quartz syenite porphyry intrusion through the contact to the wallrock, respectively (Fig. 2). The inner alteration zone, exhibiting common alteration and mineralization characteristics of porphyry Cu–Mo system, is shown by K-silicate and quartz-sericite alterations of the intrusion, and generally accompanied by abundant spot- and veinlet-disseminated molybdenite and relatively minor veinlet-disseminated chalcopyrite mineralization. The skarn zone, in the contact between the intrusion and the wallrock of the middle Silurian limestone and sandstone, is characterized by the mineral assemblage of garnet, scapolite, tremolite, epidote, diopside and forsterite, and generally accompanied by abundant massive and disseminated Cu-sulfide and massive magnetite mineralization. The outer alteration zone located in the wallrock is mainly composed of marble, with local serpentinitization, silicification, chloritization, wollastonitization and clinohumitization, exhibiting local weak Pb–Zn- and Cu–Mo-mineralization near the skarn zone (No. 15 Geological Survey Team of Yunan Geological Bureau, 1973).

3. Sampling and analytical methods

3.1. He and Ar isotopic analyses

The samples determined in this study are pyrites in ores from inner alteration zone of the Tongchang deposit. Pyrites, used for He and Ar isotopic determinations, are all perfect in crystal-morphology and coarse-grained. The ore samples were first crushed, and then the pyrite separates were hand-picked under a binocular microscope in order to remove impurities.

He and Ar isotopic compositions of inclusion-trapped fluids from six pyrite samples were measured with an all-metal extraction line and mass spectrometer (GV 5400) at the State Key Laboratory of Ore Deposit Geochemistry, Institute of Geochemistry, Chinese Academy of Sciences. The sensitivities of GV5400 for He and Ar were 3.9725×10^{-4} A/Torr and 1.1018×10^{-3} A/Torr, respectively, and the resolutions for High Mass Faraday and Multiplier were 228.1 and 628.3, respectively. The analytical methods in the present study are similar to those described by Li et al. (2011) and Hu et al. (2012). Approximately 500–1000 mg of coarse-grained pyrite separates were cleaned ultrasonically in acetone, dried, and then loaded into on-line in vacuum crusher buckets. The samples were baked at 120–150 °C in the crusher buckets for ca. 24 h to remove adhered atmospheric gases, then pumping the crusher buckets down to a high-vacuum system. The gases from fluid inclusions were released by sequential crushing the pyrite grains in high-vacuum conditions (10^{-8} Torr), and then loaded into the gas purification systems in order to purify the released gases. He was separated from Ar using an activated charcoal cold finger at liquid N_2 temperature (−196 °C) for 40–60 min to trap Ar. The isotopes and abundances of He and Ar were measured on the GV 5400 with analytical errors <10%. Gas abundances were measured by peak-height comparison with known amounts of standard air from an air bottle. He and Ar abundances and isotopic ratios were calibrated against pipettes of 0.1 cm^3 STP air (5.2×10^{-7} cm^3 STP ^{4}He and 9.3×10^{-4} cm^3 STP ^{40}Ar). Procedural blanks were $<2 \times 10^{-10}$ cm^3 STP ^{4}He and $(2–4) \times 10^{-10}$ cm^3 STP ^{40}Ar, and constituted <1% of analyses. The blank is too low to affect calibration of the abundance measurement. Crushing weight was the weight of samples smaller than 100 meshes. Four of the six samples were crushed twice in order to get enough gases from fluid inclusions (Hu et al., 1998).

3.2. Sulfur isotopic analysis

The samples used for sulfur isotopic determination are pyrites and chalcopyrites from the inner alteration zone of the Tongchang

deposit. Pyrite- and chalcopyrite-bearing ore samples were first crushed, and then the pyrite and chalcopyrite separates were hand-picked under a binocular microscope in order to remove impurities. The pyrite and chalcopyrite separates were crushed into powder of 200 meshes without pollution in an agate mortar after ultrasonically cleaning and drying. The sulfide powder was enclosed in a tin cup, and then put into the reacting furnace. Subsequently, the powder was changed into SO_2. Helium as a carrier gas mixed with the SO_2 was transported into the Mass Spectrometer. The sulfur isotopic determination was performed on a Continued Flow Isotope Ratio Mass Spectrometer (CF-IRMS) (EA-IsoPrime; EA: Euro 3000; IRMS: GVinstruments) at the State key Laboratory of Environmental Geochemistry, Institute of Geochemistry, Chinese Academy of Sciences. The standards of GBW 04415 and GBW 04414 (Ag_2S) were used for analytical quality control. The analytical procedure usually yielded an in-run precision of ±0.1‰ (2σ). The calibrations were performed with regular analyses of internal $\delta^{34}S_{CDT}$ (CDT: Canyon Diablo Troilite) standard samples.

4. Results

4.1. He and Ar isotopes of the Tongchang deposit

The measured He and Ar isotopic compositions of inclusion-trapped fluids in pyrites from the Tongchang deposit are listed in Table 2. The results show that ^4He ranges from 2.23×10^{-7} to 5.98×10^{-6} cm^3 STP g^{-1}, ^{40}Ar from 4.19×10^{-7} to 1.14×10^{-6} cm^3 STP g^{-1}, $^3He/^4He$ from 0.17 ± 0.01 to 1.50 ± 0.09 Ra and $^{40}Ar/^{36}Ar$ from 299.1 ± 15.9 to 347.3 ± 19.6.

4.2. Sulfur isotope of the Tongchang deposit

The analytical results of sulfur isotopic compositions of pyrites and chalcopyrites from the Tongchang deposit are presented in Table 3. The $\delta^{34}S$ values of the sulfides range from 1.0‰ to 1.5‰ with an average of 1.2‰. The $\delta^{34}S$ values of 10 pyrite samples vary from 1.0‰ to 1.5‰ with an average of 1.2‰, whereas the $\delta^{34}S$ values of 6 chalcopyrite samples range from 1.0‰ to 1.3‰ with an average of 1.1‰.

5. Discussion

5.1. He, Ar and S isotopic compositions of the Tongchang deposit and their geological implications

5.1.1. Examination of He and Ar isotopic data validity of the Tongchang deposit

Whether the measured He and Ar isotopes of fluid inclusions reflect the original fluid composition depends on the extent of modifications by post-entrapment processes which may include addition of cosmogenic ^3He and in situ produced ^4He and ^{40}Ar, and He loss, etc. (Hu et al., 2012), thus to examine these modifications is rather necessary in order to well constrain the origins of the ore-forming fluids.

Pyrite is considered to be a suitable mineral for trap of noble gases (Stuart et al., 1994; Baptiste and Fouquet, 1996; Hu et al., 1998, 2004; Burnard et al., 1999; Li et al., 2007; Sun et al., 2009; Wu et al., 2011). He and Ar compositons of inclusion-trapped fluids in pyrites are unlikely to be extensively lost within 100 million years (Baptiste and Fouquet, 1996). Even though the trapped He and Ar are partially lost, the ratios of $^3He/^4He$ and $^{40}Ar/^{36}Ar$ can still remain unchanged (Baptiste and Fouquet, 1996; Hu et al., 1998, 1999, 2004; Ballentine and Burnard, 2002). Given that the Tongchang deposit has a mineralization age of ca. 34 Ma (Xu et al., 2012), the loss of He and Ar is relatively limited and cannot induce notable influence on the He and Ar isotopic compositions. The pyrite samples used in this study are all from underground workings, thus the cosmogenic ^3He could be eliminated (Simmons et al., 1987; Stuart et al., 1995). The nuclear decay of Li, U and Th can produce ^4He. Because pyrite is not a Li-bearing mineral, the measured He isotopic compositions should not be influenced by nuclear decay of Li (Ballentine and Burnard, 2002). After the trap of fluid inclusions, the in situ produced ^4He from nuclear decay of U and Th, in lattice of host pyrites, cannot diffuse into the fluid inclusions (Simmons et al., 1987; Stuart and Turner, 1992; Stuart et al., 1995). Even though the fluids are released from fluid inclusions by crushing the host minerals, the ^4He from nuclear decay of U and Th, in lattice of host minerals, cannot be released (Stuart and Turner, 1992). Moreover, the hydrothermal fluids usually contain very low concentrations of U and Th (Norman and Musgrave, 1994), and even do not contain Th (Hu et al., 1999). The estimation by Hu et al. (1999) indicated that the in situ produced ^4He by nuclear decay of 3 ppm U (possibly much higher than U concentrations of the actual geological fluids) in inclusion-trapped fluids, within 50 million years, could not induce notable influence on the $^3He/^4He$ ratios. Therefore, the in situ produced ^4He by nuclear decay of U in inclusion-trapped fluids, in the Tongchang deposit with a mineralization age of ca. 34 Ma, could not exert notable influence on the $^3He/^4He$ ratios. The in situ produced ^{40}Ar from mineral lattice and fluid inclusions are thought to be negligible due to low diffusivity of Ar in pyrite (York et al., 1982; Smith et al., 2001) and the extremely low K concentration in pyrite (York et al., 1982). The pyrites measured in this study are all perfect in crystal-morphology and coarse-grained, and no cracks were found in pyrites under binocular. Moreover, the fluid inclusions in quartz veins, formed together with the pyrites, were mostly vapor-rich, CO_2-rich and daughter mineral-bearing primary fluid inclusions. Therefore, the fluid inclusions in pyrites should be the primary fluid inclusions. As a result, the measured values of He and Ar abundances and isotopic compositions of the pyrite samples should represent the characteristics of original ore-forming fluids of the deposit.

5.1.2. He and Ar isotopic compositions of the Tongchang deposit and their geological implications

Noble gases in inclusion-trapped fluids have three potential sources, i.e., notably air-saturated water, mantle-derived fluids and crust-derived fluids (Turner et al., 1993a,b; Stuart et al., 1995). Noble gases in inclusion-trapped fluids are usually considered to be a combination of different proportions of these three end-members. Pure air-saturated water (PASW) (meteoric or marine) is similar to atmospheric He and Ar isotope compositions with $^{40}Ar/^{36}Ar = 295.5$ and $^3He/^{36}Ar = 5 \times 10^{-8}$ (Turner et al., 1993a,b; Stuart et al., 1995; Burnard et al., 1999). He in the atmosphere is too low to exert a significant influence on He abundances and isotopic compositions of most crustal fluids (Marty et al., 1989; Stuart et al., 1994). This can be seen from the F^4He value, defined as the $^4He/^{36}Ar$ ratio of the sample relative to the atmospheric $^4He/^{36}Ar$ value of 0.1655. Samples used in this study have the F^4He values ranging from 334 to 11,746, with an average of 3314, which are much higher than 1, indicating the ore-forming fluids of the Tongchang deposit contain negligible atmospheric He. Therefore, mantle-derived He and radiogenic He produced in the crust are two more possible sources of He in the ore-forming fluids of the Tongchang deposit (Turner et al., 1993a,b). The crust and subcontinental mantle have $^3He/^4He$ characteristic ratios of 0.01–0.05 Ra and 6–7 Ra, respectively (Mamyin and Tolstikhin, 1984; Turner et al., 1993a,b; Dunai and Baur, 1995; Ballentine and Burnard, 2002). The $^3He/^4He$ ratios (0.17–1.50 Ra) of the ore-forming fluids of the Tongchang deposits are much higher than those of the crust, but

Table 2
He and Ar isotopic compositions of inclusion-trapped fluids in pyrites from the Tongchang, Machangqing and Yulong deposits.

Deposit	Sample no.	Sampling location	Sample description	Crushing number	Weight (g)	$^4He/cm^3$ STP	$^3He/cm^3$ STP	$^{40}Ar/cm^3$ STP	$^3He/^4He$ (Ra)	$^{40}Ar/^{36}Ar$	$^{40}Ar^*/^4He$	$^4He/cm^3$ STP g^{-1}	$^{40}Ar/cm^3$ STP g^{-1}
Tongchang	TCD0802	Inner alteration zone	Pyrite-bearing quartz veins	1	0.2162	2.35E−07	3.05E−13	9.48E−08	0.93 ± 0.05	347.3 ± 19.6	0.0602 ± 0.0041	1.09E−06	4.38E−07
	TCD0808			1		3.33E−08	7.01E−14	8.99E−08	1.50 ± 0.09	309.3 ± 16.1	0.0275 ± 0.0017		
				2		4.77E−08	7.96E−14	9.82E−08	0.19 ± 0.06	315.2 ± 16.6	0.0190 ± 0.0012		
				Total	0.1995	8.10E−08	1.50E−13	1.88E−07	1.32 ± 0.10	312.3 ± 23.2	0.0228 ± 0.0020	4.06E−07	9.43E−07
	TC0809-1			1		3.68E−08	3.45E−14	1.99E−07	0.67 ± 0.04	299.1 ± 15.9	0.0121 ± 0.0007		
				2		4.25E−08	2.88E−14	1.08E−07	0.49 ± 0.03	303.5 ± 15.7	0.0258 ± 0.0018		
				Total	0.3078	7.93E−08	6.34E−14	3.08E−07	0.57 ± 0.05	300.6 ± 22.3	0.0156 ± 0.0014	2.58E−07	9.99E−07
	TC0812			1		1.02E−06	2.50E−13	1.68E−07	0.17 ± 0.01	319.0 ± 16.0	0.0658 ± 0.0041		
				2		3.56E−07	1.71E−13	9.42E−08	0.34 ± 0.02	327.5 ± 19.2	0.1201 ± 0.0076		
				Total	0.2307	1.38E−06	4.20E−13	2.62E−07	0.22 ± 0.02	322.0 ± 24.8	0.1284 ± 0.0082	5.98E−06	1.14E−06
	TCD0816		Quartz-sericite alteration porphyries with pyrite + chalcopyrite + molybdentite mineralizations	1		1.38E−07	4.18E−14	1.36E−07	0.22 ± 0.01	304.0 ± 15.4	0.1250 ± 0.0113		
				2		1.72E−07	4.66E−14	1.17E−07	0.19 ± 0.01	304.0 ± 15.4	0.0650 ± 0.0042		
				Total	0.2718	3.10E−07	8.84E−14	2.53E−07	0.20 ± 0.02	304.0 ± 21.8	0.0674 ± 0.0043	1.14E−06	9.32E−07
	TCD0817			1	0.2515	5.61E−08	5.18E−14	1.05E−07	0.66 ± 0.04	306.2 ± 15.2	0.0663 ± 0.0060	2.23E−07	4.19E−07
Machangqing	HM60	Orebody	Pyrite-bearing hydrothermal quartz veins	1		4.20E−14	8.99E−14	1.23E−07	1.6 ± 0.1	316.7 ± 2.5	0.24 ± 0.02		
				2		5.40E−09	1.53E−14	5.70E−09	1.7 ± 0.1	436.4 ± 21.5	0.36 ± 0.04		
				3		4.20E−09	1.23E−14	5.80E−09	2.1 ± 0.1				
				Total	0.1136	4.80E−08	2.75E−14	1.29E−07	1.6 ± 0.1	320.6 ± 2.5	0.25 ± 0.02	4.20E−07	1.10E−06
	HM7			1		7.51E−08	1.69E−13	1.61E−07	1.6 ± 0.1	331.1 ± 2.5	0.27 ± 0.02		
				2		4.97E−08	1.03E−13	5.10E−08	1.5 ± 0.1	373.7 ± 3.7	0.23 ± 0.02		
				Total	0.1093	1.25E−07	2.72E−13	2.12E−07	1.6 ± 0.1	342.1 ± 2.5	0.25 ± 0.02	1.14E−06	1.90E−06
	HM72			1		1.28E−08	2.70E−14	1.10E−08	1.5 ± 0.1	428.7 ± 16.0	0.28 ± 0.03		
				2		2.60E−09	6.90E−15	1.60E−09	1.9 ± 0.2				
				Total	0.1048	1.50E−08	3.39E−14	1.30E−08	1.6 ± 0.1			1.50E−07	1.00E−07
	HM73			1		5.08E−08	1.21E−13	6.60E−08	1.7 ± 0.1	346.1 ± 3.7	0.21 ± 0.02		
				2		1.33E−08	3.52E−14	1.10E−08	1.9 ± 0.1	397.8 ± 17.5	0.23 ± 0.02		
				Total	0.112	6.40E−08	1.56E−13	7.70E−08	1.7 ± 0.1	352.9 ± 4.0	0.21 ± 0.02	5.70E−07	6.00E−07
	HM52			1		7.10E−09	8.81E−15	1.20E−08	0.9 ± 0.1	341.1 ± 6.5	0.25 ± 0.02		
				2		2.24E−08	3.46E−14	1.70E−08	1.1 ± 0.1	360.7 ± 7.7	0.15 ± 0.01		
				Total	0.0552	3.00E−08	4.34E−14	2.90E−08	1.1 ± 0.1	352.2 ± 5.4	0.17 ± 0.02	5.30E−07	5.00E−07
	HM15			1		6.36E−09	4.03E−15	9.20E−09	0.9 ± 0.2	320.5 ± 14.3	0.13 ± 0.01		
				2		2.33E−09	2.68E−14	2.30E−09	0.8 ± 0.1				
				Total	0.0254	8.69E−09	3.09E−14	1.10E−08	0.9 ± 0.1			3.40E−07	4.00E−07
	HM11			1	0.0221	1.45E−08	1.05E−14	9.60E−09	0.5 ± 0.1	339.7 ± 4.6	0.09 ± 0.01	6.60E−07	4.00E−07
Yulong	PD8-1	Orebody	Pyrite-bearing hydrothermal quartz veins	1		5.26E−08	4.75E−14	5.3E−08	0.65 ± 0.06	422.7 ± 17.8	0.3 0 ± 0.03		
				2		9.10E−08	5.31E−14	3.84E−08	0.42 ± 0.04	388.2 ± 15.3	0.10 ± 0.01		
				3		6.66E−08	4.81E−14	2.87E−08	0.52 ± 0.05	361.6 ± 13.4	0.08 ± 0.01		
				Total	0.0922	2.10E−07	1.49E−13	6.71E−08	0.46 ± 0.03	376.4 ± 10.3	0.09 ± 0.01	1.71E−06	7.28E−07
	ZK59-16			1		5.08E−08	1.12E−13	4.73E−08	1.58 ± 0.13	455.6 ± 17.3	0.32 ± 0.02		
				2		3.51E−08	5.03E−14	*n*	1.03 ± 0.09				
				3		2.49E−08	2.73E−14	*n*	0.79 ± 0.09				
				Total	0.0966	1.11E−07	1.89E−13		1.23 ± 0.07			1.15E−06	
	ZK59-11			1		5.20E−08	1.08E−13	1.52E−07	1.50 ± 0.12	315.6 ± 14.3	0.18 ± 0.06		
				2		2.27E−08	4.45E−14	4.01E−08	1.41 ± 0.13	414.8 ± 16.3	0.51 ± 0.04		
				Total	0.1134	7.46E−08	1.53E−13	1.92E−07	1.47 ± 0.09	332.2 ± 12.6	0.28 ± 0.04	6.58E−07	1.69E−06
	W81			1		2.40E−07	1.50E−13	1.08E−07	0.45 ± 0.14	630.1 ± 24.7	0.24 ± 0.01		
				2		8.27E−08	7.36E−14	4.15E−08	0.64 ± 0.04	643.0 ± 26.5	0.27 ± 0.02		
				Total	0.0571	3.23E−07	2.24E−13	1.50E−07	0.50 ± 0.03	633.6 ± 18.9	0.25 ± 0.01	5.66E−06	2.62E−06
	W4			1		1.86E−07	4.08E−13	1.97E−07	1.58 ± 0.12	377.8 ± 23.3	0.23 ± 0.03		
				2		1.07E−07	2.26E−13	9.98E−08	1.52 ± 0.12	376.2 ± 15.3	0.20 ± 0.02		
				3		3.71E−08	7.79E−14	3.32E−08	1.51 ± 0.14	404.7 ± 16.0	0.24 ± 0.02		
				4		3.21E−08	4.91E−14	1.61E−08	1.10 ± 0.09	515.7 ± 20.2	0.21 ± 0.01		
				5		7.26E−08	1.45E−13	4.05E−08	1.44 ± 0.11	370.7 ± 14.4	0.11 ± 0.01		
				Total	0.0804	4.35E−07	9.07E−13	3.87E−07	1.50 ± 0.06	383.0 ± 13.0	0.20 ± 0.01	5.42E−06	4.81E−06

Data of the Tongchang, Machangqing and Yulong deposits are from this study, Hu et al. (1998) and Hu et al. (2004), respectively.
Ra: $^3He/^4He$ ratio of air; $^{40}Ar^*$ refers to the excess Ar; Errors quoted are at the 1σ confidence level; Totals are the sums of all crushes; *n*: under determination limit.

Table 3
Sulfur isotopic compositions of hydrothermal sulfides from the Tongchang deposit.

Sample no.	Sampling location	Sample description	Mineral measured	$\delta^{34}S_{CDT}$ (‰)
TCD0802	Inner alteration zone	Pyrite-bearing	Pyrite	1.2
TC0805-2		quartz veins	Pyrite	1.2
TC0805-3			Pyrite	1.5
TCD0808			Pyrite	1.4
TC0809-1			Pyrite	1.2
TCD0811			Pyrite	1.5
TC0812			Pyrite	1.1
TC0813		Quartz-sericite alteration porphyries with pyrite +	Pyrite	1.1
TCD0816		chalcopyrite + molybdentite mineralizations	Pyrite	1.0
TCD0817			Pyrite	1.2
TC0906			Chalcopyrite	1.1
TC0907			Chalcopyrite	1.3
TC0926			Chalcopyrite	1.0
TC0927			Chalcopyrite	1.0
TC0929			Chalcopyrite	1.3
TC0930			Chalcopyrite	1.1

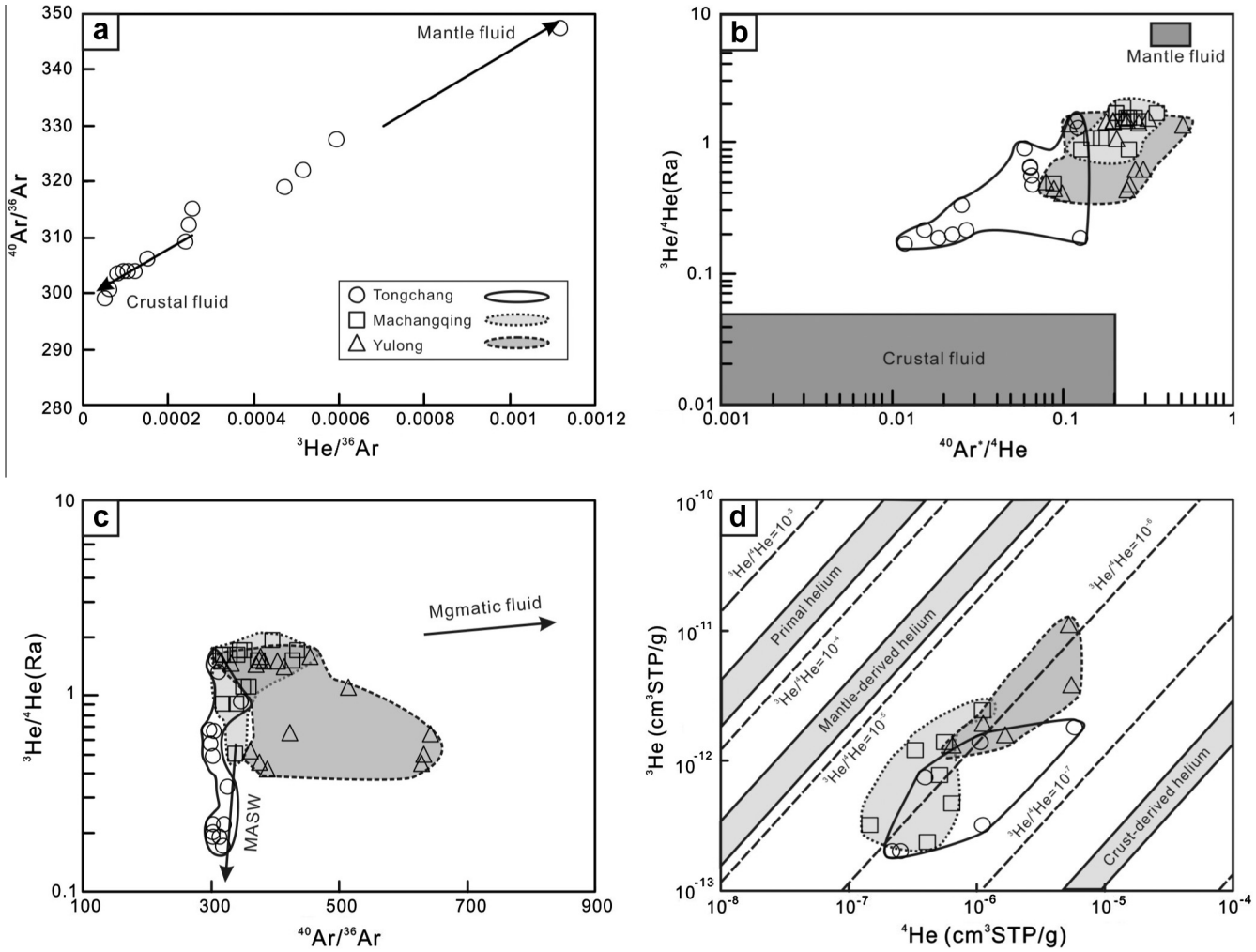

Fig. 3. (a) $^{3}He/^{36}Ar$–$^{40}Ar/^{36}Ar$ plot of inclusion-trapped fluids in pyrites from the Tongchang deposit; (b) $^{40}Ar^{*}/^{4}He$–$^{3}He/^{4}He$ plot of inclusion-trapped fluids in pyrites (modified from Hu et al., 2012); (c) $^{40}Ar/^{36}Ar$–$^{3}He/^{4}He$ plot of inclusion-trapped fluids in pyrites; (d) Helium isotopic compositions of inclusion-trapped fluids in pyrites. Data of He and Ar isotopes from Table 2.

lower than those of the subcontinental mantle, demonstrating that the ore-forming fluids contain mantle- and crust-derived He. A notable positive correlation between He and Ar isotopic compositions can be seen in the Fig. 3a and b. This positive correlation suggests that the noble gases in the ore-forming fluids of the Tongchang deposit are probably a mixture between a high $^{3}He/^{4}He$ and $^{40}Ar/^{36}Ar$ mantle-derived fluid, and a low $^{3}He/^{4}He$ and $^{40}Ar/^{36}Ar$ crust-derived fluid. This situation is similar to those for the Machangqing and Yulong deposits (Hu et al., 1998, 2004).

5.1.2.1. Crust-derived fluid. The crust-derived fluids trapped in inclusions in pyrite crystals probably contain radiogenic ^{4}He and

(to a lesser extent) radiogenic ^{40}Ar. The $^{3}He/^{36}Ar$ of the crust-derived fluid cannot be changed because both ^{3}He and ^{36}Ar are not radiogenic. Therefore, it is possible to estimate the $^{40}Ar/^{36}Ar$ for the crust-derived fluid end-member by extrapolating the trend in Fig. 3a to the $^{3}He/^{36}Ar$ value of PASW (5×10^{-8}). The estimated $^{40}Ar/^{36}Ar$ for the crust-derived fluid end-member for the Tongchang deposit is 299.5, which is close to the Ar isotopic composition of PASW ($^{40}Ar/^{36}Ar \approx 295.5$) plus very little radiogenic ^{40}Ar ($^{40}Ar^{*}$; $^{40}Ar^{*}$ is calculated assuming that all ^{36}Ar is atmospheric in origin, i.e., $^{40}Ar^{*} = {}^{40}Ar - [{}^{36}Ar \times 295.5]$) derived either from crustal rocks or from ^{40}Ar produced by in situ decay of ^{40}K (Stuart et al., 1995; Ballentine et al., 2002). Similarly, the estimated $^{3}He/^{4}He$ for the crust-derived fluid end-member for the Tongchang deposit is close to 0 Ra by extrapolating the trend in Fig. 3 to $^{40}Ar^{*}/^{4}He$ value of 0. This value is much lower than the value of PASW ($^{3}He/^{4}He$ = 1 Ra), but close to the crustal value (<0.05 Ra), indicating the presence of radiogenic ^{4}He derived from crustal rocks or from ^{4}He produced by in situ decay of U and Th (Ballentine et al., 2002). The above-mentioned investigation indicate that the crust-derived fluid end-member of the ore-forming fluids of the Tongchang deposit represents a fluid with characteristics of near atmospheric Ar and crustal He [here described as "modified air-saturated water" (MASW)] (Hu et al., 1998, 2004).

When $^{3}He/^{4}He$ ratio is lower than 0.05 Ra (characteristic values of the crust), a $^{40}Ar^{*}/^{4}He$ ratio of ca. 0.0016–0.0061 is obtained from the trend between $^{3}He/^{4}He$ and $^{40}Ar^{*}/^{4}He$ ratios (Fig. 3b), notably lower than the estimated instantaneous $^{40}Ar^{*}/^{4}He$ production ratio of the crust (≈0.2; Torgersen et al., 1988; Ballentine and Burnard, 2002). The low $^{40}Ar^{*}/^{4}He$ ratios are attributed to preferential acquisition of ^{4}He over ^{40}Ar from aquifer rocks (Torgersen et al., 1988), due to the higher closure temperature of Ar (250 °C) relative to He (<200 °C) in most minerals (Lippolt and Weigel, 1988; McDougall and Harrison, 1988; Torgersen et al., 1988; Elliot et al., 1993; Ballentine and Burnard, 2002). The proportion of $^{40}Ar^{*}$ can be estimated using the following equation (Kendrick et al., 2001):

$$^{40}Ar^{*}\% = \frac{(^{40}Ar/^{40}Ar)_{sample} - 2955}{(^{40}Ar/^{40}Ar)_{sample}} \times 100$$

The estimated proportions of $^{40}Ar^{*}$ range from 1.2% to 14.9% with an average of 5.3%. Correspondingly, the proportions of air-derived ^{40}Ar vary from 85.1% to 94.4% with an average of 98.8%.

5.1.2.2. Mantle-derived fluid. High $^{3}He/^{4}He$ and $^{40}Ar/^{36}Ar$ ratios are notable characteristics of mantle-derived fluids (Turner et al., 1993a,b; Stuart et al., 1995). Hence, the only plausible source of the end-member with high $^{3}He/^{4}He$ and $^{40}Ar/^{36}Ar$ ratios, as reflected by Fig. 3a and b, is derived from the mantle. Extrapolating the trend in Fig. 3b to a likely mantle $^{3}He/^{4}He$ ratio of 6–7 Ra (the $^{3}He/^{4}He$ ratios of subcontinental mantle; Dunai and Baur, 1995; Gautheron and Moreira, 2002) implies a $^{40}Ar^{*}/^{4}He$ ratio of 0.54–0.63. The ratio is generally similar to $^{40}Ar^{*}/^{4}He$ ratio of the subcontinent mantle (0.33–0.56; Burnard et al., 1998). Using a value of 6.5 Ra to represent mantle-derived He, and 0.03 Ra for crust-derived fluids, the estimated proportion of mantle-derived He ranges from 2% to 23% with an average of 8%, indicating a minority of mantle-derived fluid participation in ore-forming fluids for the Tongchang deposit.

Transport of fluids from the magma into the hydrothermal system cannot significantly induce fractionation between He and Ar (Graham, 2002; Hu et al., 2004). Thus, the lack of He–Ar fractionation implies efficient transfer of magmatic volatiles into the hydrothermal system (Hu et al., 2004). The transport of mantle volatiles through the crust is closely related to tectonic setting. Mantle ^{3}He in crustal fluids is generally found in crustal extension backgrounds, thought to be released during intrusion of subsurface mantle-derived melts associated with extension (Oxburgh et al., 1986; Ballentine and Burnard, 2002; Hu et al., 2004). As described above, the Tongchang deposit is genetically associated with the Tongchang alkaline quartz syenite porphyry intrusions formed in a strike-slip extension tectonic setting (Wang et al., 2004; Hou et al., 2006, 2007a; Xu et al., 2012), i.e., the ore-forming fluids of the Tongchang deposit were mainly derived from the differentiated fluids by magmatic crystallization. A previous study indicated that the quartz syenite porphyries of the Tongchang deposit were derived from an enriched mantle (EMII) source (Xu et al., 2011). Thus, the mantle-derived fluid end-member in the ore-forming fluid of the Tongchang deposit was most probably related to the mantle-derived quartz syenite porphyry rocks, most likely representing a high temperature magmatic fluid (Fig. 3c).

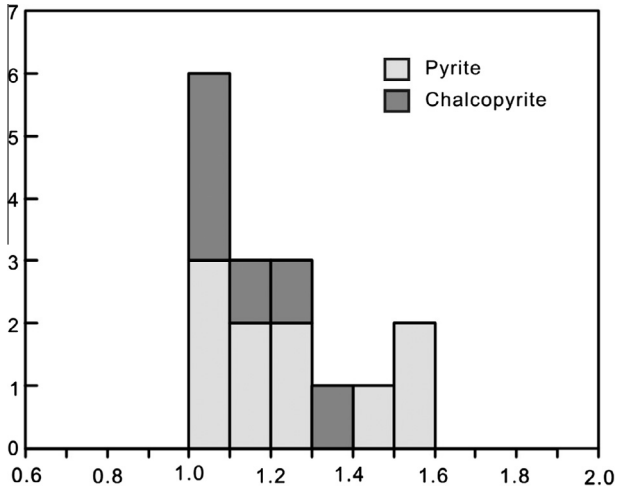

Fig. 4. $\delta^{34}S$ frequency chart of hydrothermal sulfides from the Tongchang deposit (the data from Table 3).

5.1.3. Sulfur isotopic composition of the Tongchang deposit and its geological implications

The $\delta^{34}S$ values of 10 pyrite samples vary from 1.0‰ to 1.5‰ with an average of 1.2‰, similar to the $\delta^{34}S$ values of six chalcopyrite samples ranging from 1.0‰ to 1.3‰ with an average of 1.1‰ (Table 3 and Fig. 4). The average $\delta^{34}S$ value of the pyrite samples are higher than that of the chalcopyrite samples, suggestting that a sulfur isotopic fractionation equilibrium had been reached (Ohmoto, 1972; Ohmoto and Rye, 1979; Wei and Wang, 1988). Without the existence of sulfate minerals, the $\delta^{34}S$ values of pyrites can approximately represent the total $\delta^{34}S$ values of the ore-forming fluids (Ohmoto, 1972; Ohmoto and Rye, 1979). Given that the sulfate minerals did not appear in ore rocks of the Tongchang deposit, the low $\delta^{34}S$ values and narrow $\delta^{34}S$ scopes of the pyrite samples indicate that the sulfur of the ore-forming fluids of the Tongchang deposit was derived from a homogeneous magmatic source. A previous study by Xie et al. (1984) revealed that five magmatic pyrite samples from the ore-bearing quartz syenite porphyries of the Tongchang deposit had $\delta^{34}S$ values ranging from 0.5‰ to 1.8‰ with an average of 1.1‰, exhibiting a feature of mantle-derived or magmatic sulfur (0 ± 2‰) (Seal, 2006). The $\delta^{34}S$ values of the hydrothermal pyrite samples are consistent with those of magmatic pyrite samples from the ore-bearing quartz syenite porphyries at the Tongchang deposit, suggesting that the sulfur in the ore-forming fluids was primarily derived from the ore-bearing quartz syenite porphyry magma. As the Tongchang ore-bearing quartz syenite porphyries originated from an enriched mantle (Xu et al., 2011), we can conclude that the sulfur in the ore-forming fluids should be ultimately derived from the mantle.

5.2. Genetic implications of He, Ar and S isotopes for the Tongchang deposit

It is clear that the ore-forming fluids for the Tongchang deposit are a mixture between a crust-derived fluid (MASW, with near atmospheric Ar and crustal He) and a mantle-derived fluid. The characteristics imply that mantle- and crust-derived components are both involved in the formation of the Tongchang deposit. This is consistent with a previous study by Xu et al. (2011), i.e., the Tongchang ore-bearing quartz syenite porphyry magma was derived from an enriched mantle source (EMII), and this mantle source had experienced the assimilation of subducted oceanic crust. As demonstrated above, the mantle end-member in the ore-forming fluids was most probably directly from exsolution of the mantle-derived quartz syenite porphyry magma at the Tongchang deposit. However, for the crust-derived fluid (MASW), this can be explained by mixing between a pure air-saturated water with atmospheric Ar, and an exsolved fluid from the Tongchang quartz syenite porphyry magma. As described above, the source of the Tongchang quartz syenite porphyry magma had experienced crustal assimilation. As a result, the exsolved fluids from the Tongchang quartz syenite porphyry magma should have crustal He. When the exsolved fluids were mixed with the pure air-saturated water, the crust-derived fluids (MASW), with near atmospheric Ar and crustal He, were formed. However, a possible interaction between the mixed fluids and crustal wallrock could not be ignored due to fluid convection at crustal level. As mentioned above, the sulfur in the ore-forming fluids of the Tongchang deposit was primarily derived from the magma or indirectly mantle-derived without assimilation of crustal sulfur.

5.3. Possible differences of ore-forming fluids between the Yulong, Machangqing and Tongchang porphyry Cu–Mo deposits

As shown above, significant differences, including magmatic sources, magmatic emplacement and ore-forming ages, mineralization scales and metal grades (Table 1; Hu et al., 2004; Hou et al., 2006, 2007c; Xu et al., 2011, 2012), exist between the Yulong, Machangqing and Tongchang porphyry Cu–Mo deposits. The He and Ar isotopes of the ore-forming fluids from the Yulong and Machangqing deposits had been determined (Table 2) and systematically studied by Hu et al. (1998, 2004), combined with the new noble gas data of the Tongchang deposit, which provides an opportunity to investigate possible differences of the ore-forming fluids among the Yulong, Machangqing and Tongchang porphyry Cu–Mo deposits, and further understand the mechanisms of the porphyry Cu–Mo mineralization in the Jinshajiang–Red River alkaline igneous belt.

As deduced from Fig. 3b–d, although the He and Ar isotope compositions of the three deposits follow the approximately similar trends, the ranges for individual deposits are different. Relative to the Tongchang deposit, the ore-forming fluids of the Yulong and Machangqing deposits are obviously richer in ^{3}He and ^{40}Ar, and poorer in ^{36}Ar, i.e., the Yulong and Machangqing deposits have higher $^{3}He/^{4}He$, $^{40}Ar/^{36}Ar$ and $^{40}Ar/^{4}He$ ratios than those of the Tongchang deposit (Table 2) (Fig. 3b–d). Using values of 6.5 Ra and 0.03 Ra to represent mantle-derived He and crust-derived He, respectively, the estimated proportions of mantle-derived He for the Machangqing and Yulong deposits range from 7% to 29% with an average of 21%, and from 6% to 24% with an average of 16%, respectively, which are much higher than corresponding values of 2–23% with an average of 8% for the Tongchang deposit. These characteristics, as indicated above, suggest that the ore-forming fluids of the Yulong and Machangqing deposits could have more participation of mantle-derived fluid than the Tongchang deposit.

The participations of mantle-derived fluids during the ore-forming processes were clarified to extensively exist in various types of ore deposits, including porphyry copper deposits, epithermal gold deposits and granite-related tungsten and tin deposits, etc. (Hu et al., 1998, 2004, 2012; Li et al., 2007, 2010, 2011; Sun et al., 2009; Wu et al., 2011). Recent studies indicate that the scales of porphyry Cu deposits have a positive correlation with the contributions of mantle-derived component, as reflected by the increasing $\varepsilon_{Nd}(t)$ and $\varepsilon_{Hf}(t)$ values of the ore-bearing porphyries (Hou et al., 2007c, 2011, 2012; Xu et al., 2011). This can be attributed to the high concentrations of chalcophile elements (e.g., Cu and Au) in the mantle (Mungall, 2002; Sun et al., 2004). Given that the ore-forming fluids of these deposits were mainly differentiated from the ore-bearing magmas (Bi et al., 1999; Gu et al., 2003; Hu et al., 2004), hence, to some extent, the larger scales of the Yulong (6.5 Mt Cu @ 0.38 wt.%, 0.15 Mt Mo @ 0.04 wt.%; Xu et al., 2012) and Machangqing (0.25 Mt Cu @ 0.44 wt.% ; Xu et al., 2012) deposits than that of the Tongchang deposit are possibly connected with the more contributions of mantle-derived fluid to their ore-forming fluids.

6. Conclusions

(1) He and Ar isotopic compositions of inclusion-trapped fluids in pyrites from the Tongchang porphyry Cu–Mo deposit suggest that the ore-forming fluids are a mixture between a crust-derived fluid (MASW, with near atmospheric Ar and crustal He) and a mantle-derived fluid. The $\delta^{34}S$ values of the hydrothermal pyrite samples from the Tongchang deposit indicate that the sulfur in the ore-forming fluids of the Tongchang deposit was primarily derived from the magma or indirectly mantle-derived without assimilation of crustal sulfur.

(2) The mantle end-member for the ore-forming fluids of the Tongchang deposit was most probably directly from exsolution of the mantle-derived quartz syenite porphyry magma. However, for the crust-derived fluid (MASW, with near atmospheric Ar and crustal He), it can be explained by mixing between a pure air-saturated water with near atmospheric Ar, and an exsolved fluid with crustal He from the Tongchang quartz syenite porphyry magma, but a possible interaction between the mixed fluids and crustal wallrock could not be ignored due to fluid convection at crustal level.

(3) Compared to the Tongchang deposit, the ore-forming fluids of the Yulong and Machangqing deposits are obviously richer in ^{3}He and ^{40}Ar, and poorer in ^{36}Ar. These characteristics suggest that the ore-forming fluids of the Yulong and Machangqing deposits could have more contributions of mantle-derived fluid than the Tongchang deposit, which may be one of the most important factors producing larger scales of the Yulong and Machangqing deposits than the Tongchang deposit.

Acknowledgements

This research project is financially supported jointly by "the Key Natural Science Foundation of China (41130423), the Natural Science Foundation of China (40873037, 41203041), the 12th Five-Year Plan project of State Key Laboratory of Ore-deposit Geochemistry, Chinese Academy of Sciences (SKLOG-ZY125-06) and the Natural Science Foundation of Guizhou Province ([2012]2335)". Relevant staffs of Yunnan Honghe Henghao Mining Co. Ltd. are gratefully acknowledged for their kind help during our fieldwork. We are very grateful to Professor Hong Zhong (Institute

of Geochemistry, Chinese Academy of Sciences) and two anonymous referees for their constructive review.

References

Ballentine, C.J., Burnard, P.G., 2002. Production, release and transport of noble gases in the continental crust. Reviews in Mineralogy and Geochemistry 47, 481–538.

Ballentine, C.J., Burgess, R., Marty, B., 2002. Tracing fluid origin, transport and interaction in the crust. Reviews in Mineralogy and Geochemistry 47, 539–614.

Baptiste, P.J., Fouquet, Y., 1996. Abundance and isotopic composition of helium in hydrothermal sulfides from the East Pacific Rise at 13 N. Geochimica et Cosmochimica Acta 60, 87–93.

Bi, X.W., 1999. Study on Alkali-rich Intrusive Rocks and their Relation with Metallogenesis of Copper and Gold in the "Sanjiang" Region, Western Yunnan. Ph.D. Thesis, Institute of Geochemistry, Chinese Academy of Sciences, Guiyang (in Chinese).

Bi, X.W., Hu, R.Z., Ye, Z.J., Shao, S.X., 1999. Study on the relation between the A-type granite and Cu ore mineralization: evidence from the Machangqing copper deposit. Science in China (Series D) 29, 489–495 (in Chinese).

Bi, X.W., Cornell, D.H., Hu, R.Z., 2002. REE composition of primary and altered feldspar from the mineralized alteration zone of alkali-rich intrusive rocks, western Yunnan province, China. Ore Geology Reviews 19, 69–78.

Bi, X.W., Hu, R.Z., Cornell, D.H., 2004. Trace element and isotope evidence for the evolution of ore-forming fluid of Yao'an gold deposit, Yunnan province, China. Mineralium Deposita 39, 21–30.

Bi, X.W., Hu, R.Z., Peng, J.T., Wu, K.X., Su, W.C., Zhan, X.Z., 2005. Geochemical characteristics of the Yao'an and Machangqing alkaline-rich intrusions. Acta Petrologica Sinica 21, 113–124 (in Chinese with English abstract).

Bi, X.W., Hu, R.Z., Hanley, J.J., Mungall, J., Peng, J.T., Shang, L.B., Wu, K.X., Suang, Y., Li, H.L., Hu, X.Y., 2009. Crystallisation conditions (T, P, fO_2) from mineral chemistry of Cu- and Au-mineralised alkaline intrusions in the Red River–Jinshajiang alkaline igneous belt, western Yunnan Province, China. Mineralogy and Petrology 96, 43–58.

Burnard, P., 2012. The Noble Gases as Geochemical Tracers. Advances in Isotope Geochemistry. Springer, pp. 1–403.

Burnard, P.G., Farley, K.A., Turner, G., 1998. Multiple fluid pulses in a Samoan harzburgite. Chemical Geology 147, 99–114.

Burnard, P.G., Hu, R.Z., Turner, G., Bi, X.W., 1999. Mantle, crustal and atmospheric noble gases in Ailaoshan gold deposits, Yunnan province, China. Geochimica et Cosmochimica Acta 63, 1595–1604.

Chung, S.L., Lee, T.Y., Lo, C.H., Wang, P.L., Chen, C.Y., Yem, N.T., Hoa, T.T., Wu, G.Y., 1997. Intraplate extension prior to continental extrusion along the Ailao Shan–Red River shear zone. Geology 25, 311–314.

Chung, S.L., Lo, C.H., Lee, T.Y., Zhang, Y.Q., Xie, Y.W., Li, X.H., Wang, K.L., Wang, P.L., 1998. Diachronous uplift of the Tibetan plateau starting 40 Myr ago. Nature 394, 769–773.

Dunai, T.J., Baur, H., 1995. Helium, neon and argon systematics of the European subcontinental mantle: implications for its geochemical evolution. Geochimica et Cosmochimica Acta 59, 2767–2784.

Elliot, T., Ballentine, C.J., O'Nions, R.K., Ricchiuto, T., 1993. Carbon, helium, neon and argon isotopes in a Po basin natural gas field. Chemical Geology 106, 429–440.

Gautheron, C., Moreira, M., 2002. Helium signature of the subcontinental lithospheric mantle. Earth and Planetary Science Letters 199, 39–47.

Graham, D.W., 2002. Noble gas isotope geochemistry of mid-ocean ridge and ocean island basalts: characterization of mantle source reservoirs. Reviews in Mineralogy and Geochemistry 47, 247–317.

Gu, X.X., Tang, J.X., Wang, C.S., Chen, J.P., He, B.B., 2003. Himalayan magmatism and porphyry copper–molybdenum mineralization in the Yulong ore belt, East Tibet. Mineralogy and Petrology 78, 1–20.

Hou, Z.Q., Ma, H.W., Zaw, K., Zhang, Y.Q., Wang, M.J., Wang, Z., Pan, G.T., Tang, R.L., 2003. The Himalayan Yulong porphyry copper belt: product of large-scale strike-slip faulting in eastern Tibet. Economic Geology 98, 125–145.

Hou, Z.Q., Zeng, P.S., Gao, Y.F., Du, A.D., Fu, D.M., 2006. Himalayan Cu–Mo–Au mineralization in the eastern Indo–Asian collision zone: constraints from Re–Os dating of molybdenite. Mineralium Deposita 41, 33–45.

Hou, Z.Q., Zaw, K., Pan, G.T., Mo, X.X., Xu, Q., Hu, Y.Z., Li, X.Z., 2007a. Sanjiang Tethyan metallogenesis in SW China: tectonic setting, metallogenic epochs and deposit types. Ore Geology Reviews 31, 48–87.

Hou, Z.Q., Xie, Y.L., Xu, W.Y., Li, Y.Q., Zhu, X.K., Khin, Z., Beaudoin, G., Rui, Z.Y., Wei, H.A., Ciren, L., 2007b. Yulong deposit, eastern Tibet: a high-sulfidation Cu–Au porphyry copper deposit in the eastern Indo–Asian collision zone. International Geology Review 49, 235–258.

Hou, Z.Q., Pan, X.F., Yang, Z.M., Qu, X.M., 2007c. Porphyry Cu–(Mo–Au) deposits no related to oceanic-slab subduction: examples from Chinese porphyry deposits in continental setting. Geoscience 21, 332–351 (in Chinese with English abstract).

Hou, Z.Q., Zhang, H.R., Pan, X.F., Yang, Z.M., 2011. Porphyry Cu (–Mo–Au) deposits related to melting of thickened mafic lower crust: examples from the eastern Tethyan metallogenic domain. Ore Geology Reviews 39, 2145.

Hou, Z.Q., Zheng, Y.C., Yang, Z.M., Rui, Z.Y., Zhao, Z.D., Jiang, S.H., Qu, X.M., Sun, Q.Z., 2012. Contribution of mantle components within juvenile lower-crust to collisional zone porphyry Cu systems in Tibet. Mineralium Deposita. http://dx.doi.org/10.1007/s00126-012-0415-6.

Hu, R.Z., Burnard, P.G., Turner, G., Bi, X.W., 1998. Helium and Argon isotope systematics in fluid inclusions of Machangqing copper deposit in west Yunnan province, China. Chemical Geology 146, 55–63.

Hu, R.Z., Bi, X.W., Turner, G., Burnard, P.G., 1999. He and Ar isotopic geochemistry of the ore-forming fluids of the Ailaoshan Au ore belt. Science in China (Series D) 29, 321–330 (in Chinese).

Hu, R.Z., Burnard, P.G., Bi, X.W., Zhou, M.F., Pen, J.T., Su, W.C., Wu, K.X., 2004. Helium and argon isotope geochemistry of alkaline intrusion-associated gold and copper deposits along the Red River–Jinshajiang fault belt, SW China. Chemical Geology 203, 305–317.

Hu, R.Z., Burnard, P.G., Bi, X.W., Zhou, M.F., Peng, J.T., Su, W.C., Zhao, J.H., 2009. Mantle-derived gaseous components in ore-forming fluids of the Xiangshan uranium deposit, Jiangxi province, China: evidence from He, Ar and C isotopes. Chemical Geology 266, 86–95.

Hu, R.Z., Bi, X.W., Jiang, G.H., Chen, H.W., Peng, J.T., Qi, Y.Q., Wu, L.Y., Wei, W.F., 2012. Mantle-derived noble gases in ore-forming fluids of the granite-related Yaogangxian tungsten deposit, Southeastern China. Mineralium Deposita 47, 623–632.

Huang, B., Liang, H.Y., Mo, J.H., Xie, Y.W., 2009. Zircon LA-ICP-MS U–Pb age of the Jinping–Tongchang porphyry associated with Cu–Mo mineralization and its geological implication. Geotectonica et Metallogenia 33, 598–602 (in Chinese with English abstract).

Jiang, Y.H., Jiang, S.Y., Ling, H.F., Dai, B.Z., 2006. Low-degree melting of a metasomatized lithospheric mantle for the origin of Cenozoic Yulong monzogranite-porphyry, east Tibet: geochemical and Sr–Nd–Pb–Hf isotopic constraints. Earth and Planetary Science Letters 241, 617–633.

Kendrick, M.A., Burgess, R., Pattrick, R.A., Turner, G., 2001. Fluid inclusion noble gas and halogen evidence on the origin of Cu-porphyry mineralizing fluids. Geochimica et Cosmochimica Acta 65, 2651–2668.

Leloup, P.H., Harrison, T.M., Ryerson, F.J., Chen, W.J., Li, Q., Tapponnier, P., Lacassin, R., 1993. Structural, petrological and thermal evolution of a Tertiary ductile strike-slip shear zone, Diancang Shan, Yunnan. Journal of Geophysical Research 98, 6715–6743.

Leloup, P.H., Lacassin, R., Tapponnier, P., Scharer, U., Zhong, D.L., Liu, X.H., Zhang, L.S., Ji, S.C., Trinh, P.T., 1995. The Ailao Shan–Red River shear zone (Yunnan, China), Tertiary transform boundary of Indo–china. Tectonophysics 251, 3–84.

Leloup, P.H., Arnaud, N., Lacassin, R., Kienast, J.R., Harrison, T.M., Trong, T.T.P., Replumaz, A., Tapponnier, P., 2001. New constraints on the structure, thermochronology, and timing of the Ailao Shan–Red River shear zone, SE Asia. Journal of Geophysical Research 106, 6683–6732.

Li, Z.L., Hu, R.Z., Yang, J.S., Peng, J.T., Li, X.M., Bi, X.W., 2007. He, Pb and S isotopic constraints on the relationship between the A-type Qitianling granite and the Furong tin deposit, Hunan Province, China. Lithos 97, 161–173.

Li, X., Wang, C., Hua, R., Wei, X., 2010. Fluid origin and structural enhancement during mineralization of the Jinshan orogenic gold deposit, South China. Mineralium Deposita 45, 583–597.

Li, G., Hua, R., Zhang, W., Hu, D., Wei, X., Huang, X.e., Xie, L., Yao, J., Wang, X., 2011. He–Ar isotope composition of pyrite and Wolframite in the Tieshanlong Tungsten Deposit, Jiangxi, China: implications for fluid evolution. Resource Geology 61, 356–366.

Liang, H.Y., Campbell, I.H., Allen, C., Sun, W.D., Liu, C.Q., Yu, H.X., Xie, Y.W., Zhang, Y.Q., 2006a. Zircon Ce^{4+}/Ce^{3+} ratios and ages for Yulong ore-bearing porphyries in eastern Tibet. Mineralium Deposita 41, 152–159.

Liang, H.Y., Yu, H.X., Mo, C.H., Zhang, Y.Q., Xie, Y.W., 2006b. Zircon LA-ICP-MS U-Pb age, Ce^{4+}/Ce^{3+} ratios and the geochemical features of the Machangqing complex associated with copper deposit. Chinese Journal of Geochemestry 25, 223–229.

Lippolt, H.J., Weigel, E., 1988. ^{4}He diffusion in Ar retentive minerals. Geochimica et Cosmochimica Acta 52, 1449–1458.

Mamyin, B.A., Tolstikhin, I.N., 1984. Helium Isotopes in Nature: Amsterdam. Elsevier Publishing Company, pp. 1–273.

Marty, B., Jambon, A., Sano, Y., 1989. Helium isotope and CO_2 in volcanic gases of Japan. Chemical Geology 76, 25–40.

McDdougall, I., Harrison, T.M., 1988. Geochronology and thermochronology by the $^{40}Ar–^{39}Ar$ Method. Oxford University Press, New York, pp. 1–269.

Müller, D., Groves, D.I., 2000. Potassoic Igneous Rocks and Associated Gold–Copper Mineralization. Springer, Berlin, pp. 252.

Müller, D., Kaminski, K., Uhlig, S., Graupner, T., Herzig, P.M., Hunt, S., 2002. The transition from porphyry- to epithermal-style gold mineralization at Ladolam, Lihir Island, Papua New Guinea: a reconnaissance study. Mineralium Deposita 37, 61–74.

Mungall, J.E., 2002. Roasting the mantle: slab melting and the genesis of major Au and Au-rich Cu deposits. Geology 30, 915–918.

No. 15 Geological Survey Team of Yunan Geological Bureau, 1973. Reserve Report of Tongchang and Chang'anchong Cu–Mo Deposits in Jinping County of Yunan province, China, pp. 1–8 (in Chinese).

Norman, D.I., Musgrave, J.A., 1994. N_2–He–Ar composition in fluid inclusion: indicators of fluid source. Geochimica et Cosmochimica Acta 58, 1119–1132.

Ohmoto, H., 1972. Systematics of sulfur and carbon isotopes in hydrothermal ore deposits. Economic Geology 67, 551–578.

Ohmoto, H., Rye, R.O., 1979. Isotopes of sulfur and carbon. In: Barnes, H.L. (Ed.), Geochemistry of hydrothermal ore deposits, 2nd ed. John Wiley & Sons, New York, pp. 509–567.

Oxburgh, E.R., O'Nions, R.K., Hill, R.I., 1986. Helium isotopes in sedimentary basins. Nature 324, 632–635.

Schärer, U., Tapponnier, P., Lacassin, R., Leloup, P.H., Zhong, D.L., Ji, S.C., 1990. Intraplate tectonics in Asia: a precise age for large-scale Miocene movement

along the Ailao Shan–Red River shear zone, China. Earth and Planetary Science Letters 97, 65–77.
Schärer, U., Zhang, L.C., Tapponnier, P., 1994. Duration of strike-slip movements in large shear zones: the Red River belt, China. Earth and Planetary Science Letters 126, 379–397.
Seal, R.R., 2006. Sulfur isotope geochemistry of sulfide minerals. Reviews in Mineralogy and Geochemistry 61, 633–677.
Sillitoe, R.H., 2002. Some metallogenic features of gold and copper deposits related to alkaline rocks and consequences for exploration. Mineralium Deposita 37, 4–13.
Simmons, S.F., Sawkins, F.J., Schlutter, D.J., 1987. Mantle-derived helium in two Peruvian hydrothermal ore deposits. Nature 329, 429–432.
Smith, P.E., Evensen, N.M., York, D., Szatmari, P., Oliveira, D.C., 2001. Single-crystal ^{40}Ar–^{39}Ar dating of pyrite: no fool's clock. Geology 29, 403–406.
Stuart, F.M., Turner, G., 1992. The abundance and isotopic composition of the noble gases in ancient fluids. Chemical Geology 101, 97–109.
Stuart, F.M., Turner, G., Duckworth, R.C., Fallick, A.E., 1994. Helium isotopes as tracers of trapped hydrothermal fluids in ocean-floor sulfides. Geology 22, 823–826.
Stuart, F.M., Burnard, P.G., Taylor, R.P., Turner, G., 1995. Resolving mantle and crustal contributions to ancient hydrothermal fluids: He–Ar isotopes in fluid inclusions from Dae Hwa W-Mo mineralisation, South Korea. Geochimica et Cosmochimica Acta 59, 4663–4673.
Sun, W.D., Arculus, R.J., Kamenetsky, V.S., Binns, R.A., 2004. Release of gold-bearing fluids in convergent margin magmas prompted by magnetite crystallization. Nature 431, 975–978.
Sun, X.M., Zhang, Y., Xiong, D.X., Sun, W.D., Shi, G.Y., Zhai, W., Wang, S.W., 2009. Crust and mantle contributions to gold-forming process at the Daping deposit, Ailaoshan gold belt, Yunnan, China. Ore Geology Reviews 36, 235–249.
Tapponnier, P., Peltzer, G., Ledain, A.Y., Armijo, R., Cobbold, P., 1982. Propagating extension tectonics in Asia: new insights from simple experiments with plasticine. Geology 10, 611–616.
Torgersen, T., Kennedy, B.M., Hiyagon, H., 1988. Argon accumulation and the crustal degassing flux of ^{40}Ar in the Great Artesian Basin, Australia. Earth and Planetary Science Letters 92, 43–56.
Turner, G., Stuart, F.M., 1992. Helium/heat ratios and deposition temperatures of sulphides from the ocean floor. Nature 357, 581–583.
Turner, G., Burnard, P.B., Ford, J.L., Gilmour, J.D., Lyon, I.C., Stuart, F.M., 1993a. Tracing fluid sources and interaction: discussion. Physical Sciences and Engineering 344, 127–140.
Turner, S., Hawkesworth, C., Liu, J.Q., Rogers, N., Kelley, S., Vancalsteren, P., 1993b. Timing of Tibetan uplift constrained by analysis of volcanic rocks. Nature 364, 50–54.
Turner, S., Arnaud, N., Liu, J., Rogers, N., Hawkesworth, C., Harris, N., Kelley, S., Vancalsteren, P., Deng, W., 1996. Post-collision, shoshonitic volcanism on the Tibetan plateau: implications for convective thinning of the lithosphere and the source of ocean island basalts. Journal of Petrology 37, 45–71.
Wang, J.H., Yin, A., Harrison, T.M., Grove, M., Zhang, Y.Q., Xie, G.H., 2001. A tectonic model for Cenozoic igneous activities in the eastern Indo-Asian collision zone. Earth and Planetary Science Letters 88, 123–133.
Wang, D.H., Qu, W.J., Li, Z.W., Ying, H.L., Chen, Y.C., 2004. The metallogenic concentrating epoch of the Porphyry Copper (molybdenum) deposits in Jinshajiang–Red River metallogenic belt: Re–Os isotope dating. Science in China (Series D) 34, 345–349 (in Chinese).
Wei, J.Y., Wang, Y.G., 1988. Isotopic Geochemistry. Geological Publishing House, Beijing, pp. 153–155 (in Chinese).
Wu, L.Y., Hu, R.Z., Peng, J.T., Bi, X.W., Jiang, G.H., Chen, H.W., Wang, Q.Y., Liu, Y.Y., 2011. He and Ar isotopic compositions and genetic implications for the giant Shizhuyuan W–Sn–Bi–Mo deposit, Hunan Province, South China. International Geology Review 53, 677–690.
Xie, Y.W., Zhang, Y.Q., Hu, G.X., 1984. A preliminary study on geochemical characteristics and mineralization specificity of alkaline-rich intrusive belt in Ailaoshan–Jinshajiang. Journal of Kunming University of Science and Technology (4), 1–16 (in Chinese with English abstract).
Xu, L.L., 2011. The Diagenetic and Metallogenic Geochronology and Magmatic fO_2 Characteristics of Jinshajiang-Red River Porphyry Cu(Mo–Au) Metallogenic Systems. Ph.D. Thesis, Institute of Geochemistry, Chinese Academy of Sciences, Guiyang (in Chinese with English abstract).
Xu, L.L., Bi, X.W., Su, W.C., Qi, Y.Q., Li, L., Chen, Y.W., Dong, S.H., Tang, Y.Y., 2011. Geochemical characteristics and petrogenesis of the quartz syenite porphyry from Tongchang porphyry Cu(Mo–Au) deposit in Jinping County, Yunan Province. Acta Petrologica Sinica 27, 3109–3122 (in Chinese with English abstract).
Xu, L.L., Bi, X.W., Hu, R.Z., Zhang, X.C., Su, W.C., Qu, W.J., Hu, Z.C., Tang, Y.Y., 2012. Relationships between porphyry Cu–Mo mineralization in the Jinshajiang–Red River metallogenic belt and tectonic activity: constraints from zircon U-Pb and molybdenite Re-Os geochronology. Ore Geology Reviews 48, 460–473.
Xue, B.G., 2008. On the division of Au metallogenetic zone and metallogenetic rule in Yunnan. Yunan Geology 27, 261–277 (in Chinese with English abstract).
Yin, A., Harrison, T.M., 2000. Geologic evolution of the Himalayan–Tibetan orogen. Annual Review of Earth and Planetary Sciences 28, 211–280.
York, D., Masliwec, A., Kuybida, P., Hanes, J.E., Hall, C.M., Kenyon, W.J., Spooner, E.T.C., Scott, S.D., 1982. $^{40}Ar/^{39}Ar$ dating of pyrite. Nature 300, 52–53.
Zhang, Y.Q., Xie, Y.W., 1997. Nd, Sr isotopic character and chronology of Ailaoshan–Jinshajiang alkali-rich intrusive rocks. Science in China 27, 289–293 (in Chinese).
Zhang, Y.Q., Xie, Y.W., Tu, G.C., 1987. A preliminary study on the relationship between rift and Ailaoshan–Jianshajiang alkaline intrusive rocks. Acta Petrologica Sinica 1, 17–26 (in Chinese with English abstract).